Ultrasmall Phosphorescent Polymer Dots for Ratiometric Oxygen Sensing and Photodynamic Cancer Therapy

Huifang Shi, Xing Ma, Qiang Zhao, Bin Liu, Qiuyu Qu, Zhongfu An, Yanli Zhao, and Wei Huang**

A series of semiconducting polymer dots (Pdots) composed of phosphorescent Ir(III) complexes and polyfluorene units in the main polymer chains are designed, synthesized, and applied in ratiometric oxygen sensing and photodynamic cancer therapy. The ultrasmall Pdots with particle size less than 10 nm are fabricated in aqueous solution on account of amphiphilic nature of the polymers. The Pdots possess fine photostability, biocompatibility, and efficient energy transfer from the polymer main chain to the Ir(III) complex. By utilizing the excited-state energy transfer from phosphorescent Pdots to the ground state molecular oxygen, these Pdots are applied in the optical sensing of oxygen with ratiometric and naked-eye detection as well as high sensitivity in aqueous solution. The Pdots also show low cytotoxicity and can pass across the cell membrane to enter into the cytoplasm. The singlet oxygen photo-generated from the Pdots under irradiation at 488 nm can effectively induce the apoptosis and death of tumor cells for photodynamic cancer therapy in vitro.

1. Introduction

The past several years have witnessed the rapid development of conjugated polymer nanoparticles (CPNPs) in the chemo/biosensing and bioimaging applications,[1] as they possess combined advantages of π-conjugated polymers (CPs), such as having π-delocalized backbones and fast electron or energy transfer,[2] and nanoparticles with small particle size, fine biocompatibility and high fluorescent brightness.[3] The CPNPs could be called as polymer dots (Pdots) when they have ultrasmall particle size (less than 20 nm) and high brightness.[1b] So far, only a few studies based on the Pdots in biosensing and fluorescence imaging have been reported,[4] and most of them are non-water soluble CPs with short-lifetime fluorescent emission. In addition, the sensing and imaging performance of Pdots often suffers the interferences from the background fluorescence, such as some organic dyes in the sensing media or fluorescent bio-substrates. Thus, developing novel Pdots with high utilization efficiency is still challenging.

Phosphorescent Ir(III) complexes with high quantum efficiency, tunable luminescent color from blue to near infrared, large Stokes shift, visible excitation, excellent photostability, and long emission lifetime represent a class of promising optoelectronic materials in the family of phosphorescent transition-metal complexes.[5] All of these features endow the Ir(III) complexes as excellent candidates in optical sensing and imaging applications.[6] The long emission lifetime, above all, paves an effective way to eliminate the auto-fluorescence interferences via time-resolved photoluminescence technique[7] and fluorescence lifetime imaging microscopy,[8] which opens a unique possibility for sensing and imaging in complicated media. Thus, it is expected to introduce the Ir(III) complex into the CP main chain to obtain the phosphorescent CPNPs.[9] Recently, we reported a series of cationic conjugated polyelectrolyte materials with phosphorescent Ir(III) complexes for time-resolved luminescent heparin sensing and fluorescence lifetime imaging, in which some design principles for phosphorescent CP-based biosensors were summarized.[9a] McNeill et al.[10] also reported a two-component phosphorescent Pdot by mixing polyfluorene and platinum(II) complex PtOEP for oxygen sensing and bioimaging. However, there is still very limited research on developing phosphorescent Pdots based on single-component CPs for the applications in sensing, bioimaging, and cancer therapy.

Dr. H. F. Shi, X. Ma, Q. Qu, Prof. Y. L. Zhao
Division of Chemistry and Biological Chemistry
School of Physical and Mathematical Sciences
Nanyang Technological University
21 Nanyang Link, 637371, Singapore, Singapore
E-mail: zhaoyanli@ntu.edu.sg
Dr. H. F. Shi, Prof. W. Huang
Jiangsu-Singapore Joint Research Center for Organic/Bio-Electronics & Information Displays and Institute of Advanced Materials (IAM)
Nanjing Tech University
30 South Puzhu Road, Nanjing, P. R. China
E-mail: wei-huang@njtech.edu.cn
Prof. Q. Zhao, Z. F. An, Prof. W. Huang
Key Laboratory for Organic Electronics & Information Displays
Nanjing University of Posts and Telecommunications
210023, Nanjing, P. R. China
Prof. B. Liu
Department of Chemical and Biomolecular Engineering
National University of Singapore
4 Engineering Drive 4, 117576, Singapore, Singapore
Prof. Y. L. Zhao
School of Materials Science and Engineering
Nanyang Technological University
50 Nanyang Avenue, 639798, Singapore, Singapore

DOI: 10.1002/adfm.201400647

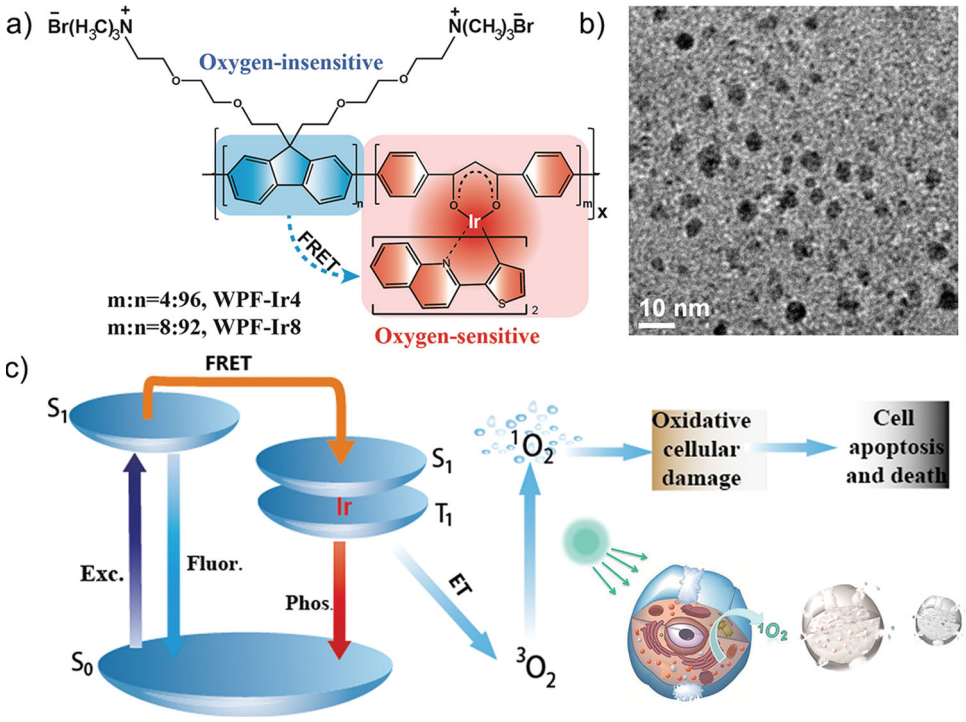

Figure 1. a) Chemical structures of phosphorescent CPs with the Ir(III) complexes; b) HR-TEM of WPF-Ir4 in aqueous solution; and c) mechanisms illustrating the oxygen sensing and PDT.

Moreover, the phosphorescent Ir(III) complexes can be utilized not only as optical sensors for oxygen because the ground state of oxygen is triplet state that can quench the triplet phosphorescence,[11] but also as photosensitizers for photodynamic therapy (PDT).[12] PDT has been developed as one of the most powerful methods in cancer therapy, which is, for certain cancers, superior to chemotherapeutic ways with systematic toxicity and long-term side effects. The photosensitizer, irradiation light, and molecular oxygen are the three primary components in the PDT process to generate reactive oxygen species (ROS) that are highly toxic to cancer cells.[13]

In this work, we report a novel class of phosphorescent CPNPs containing the Ir(III) complexes for optical oxygen sensing and photodynamic cancer therapy. Two CPs containing the Ir(III) complexes were designed and synthesized via Suzuki coupling reaction, which were composed of phosphorescent Ir(III) complexes and fluorescent flourene units as shown in **Figure 1**a. An efficient energy transfer from the polymer main chain to the Ir(III) complex occurs in this system. On account of the amphiphilic structures, these polymers could self-assemble to form phosphorescent Pdots with ultrasmall particle size of (6 ± 2) nm in aqueous solution without any further modifications and other auxiliary components (Figure 1b). By utilizing the energy transfer from the excited state of phosphorescent Pdots to the ground state of molecular oxygen (triplet state), these Pdots could be applied in the optical sensing for oxygen. Furthermore, the singlet oxygen ($^1O_2$) was produced in the energy transfer process to cause oxidative cellular damage, leading to the apoptosis and cell death to realize PDT as illustrated in Figure 1c.

2. Results and Discussion

2.1. Synthesis and Characterization

The CPs with different phosphorescent Ir(III) complex contents were obtained after the quaternization of their precursors, which were synthesized via Suzuki coupling reactions in high yields (65–75%). The synthetic routes were shown in Scheme S1 of the Supporting Information (SI). As the feed percentages of the Ir(III) complexes in the polymers were 4 and 8 mol%, the polymers are named as WPF-Ir4 and WPF-Ir8, correspondingly. These polymers were characterized by ^{1}H NMR, ^{13}C NMR and gel permeation chromatography (GPC) (see the SI). Their photophysical properties were investigated through UV-visible absorption and photoluminescent (PL) spectroscopy, and their morphologies in aqueous solution were measured by high resolution transmission electron microscopy (HR-TEM). The absorption and emission spectra of the polymers in both aqueous solution and the solid films are shown in Figure S1 of the SI. The concentrations of the polymers were calculated using the repeating units based on their feed percentages. The main absorption bands for WPF-Ir4 and WPF-Ir8 centered at 380 nm in aqueous solution (15 μM), which were assigned to the absorption of π–π^* transitions of the polymer backbones. A weak absorption band around 400–550 nm attributed to the metal-to-ligand charge-transfer (MLCT) transition of the Ir(III) complex was observed, which became much more intense in the solid films. In PL spectra, a major emission peak at 425 nm and a shoulder at 450 assigned to the polyfluorene main chain, together with a red emission peak at 630 nm due to phosphorescent Ir(III) complex, were recorded for both

polymers in aqueous solution. The red emission intensity of WPF-Ir8 is higher than that of WPF-Ir4, because of more efficient Förster resonance energy transfer (FRET) from the donor to acceptor for the polymer with higher Ir(III) complex content. This FRET phenomenon becomes more obvious in the solid state. As shown in Figure S1 of the SI, even for the WPF-Ir4 film with lower content of Ir(III) complex, the red emission at 630 nm was the dominated one and a shoulder peak at 675 nm appeared. For the WPF-Ir8 film, there was a strong red emission band at 630 nm with a shoulder. These results indicate that the aggregated state in the polymer films favors more efficient energy transfer from the polyfluorene donor to the Ir(III) acceptor.[14]

The Pdots possess the average particle size smaller than 10 nm determined by HR-TEM as shown in Figure S2a. The hydrodynamic diameter and zeta potential of the Pdots were determined by dynamic light scattering (DLS). The mean diameter of the Pdots is 19 nm and their average zeta potential is 45.9 mV (Figure S2b). It is reasonable that hydrodynamic diameter of the Pdots measured by DLS is larger than their size obtained by TEM, because the hydrodynamic diameter is the hydrated diameter combined by the Pdot cores together with the solvent coating layer, while for TEM, this hydration layer is not present. The Pdots in this work are positively charged in aqueous solution, which makes the cellular uptake of the Pdots easier through electrostatic interaction between the Pdots and negatively charged phospholipid cell membrane.

2.2. Oxygen Sensing

Next, the oxygen sensing experiments were conducted for WPF-Ir8 (as an example) in 10 mM phosphate buffered saline (PBS, pH = 7.0 at 25 °C) solution at a polymer concentration of 60 μM. The changes of PL spectra from WPF-Ir8 under various oxygen partial pressures at room temperature are revealed in **Figure 2**a. Under the nitrogen atmosphere (0% oxygen), the PL spectrum of the WPF-Ir8 solution was dominated by the triplet emission (T_1-S_0) at 630 nm with a shoulder band at 675 nm from phosphorescent Ir(III) complex, and the blue emission (S_1-S_0) at around 450 nm from the polyfluorene unit was quite weak due to the efficient FRET. The red emission intensity of the polymer solution around 630 nm, however, decreased remarkably with an enhancement of the oxygen pressure, and quenched at 100% oxygen atmosphere. The emission color of the solution changed from red to blue upon the increase of the oxygen pressure, which could be visualized by naked eyes under a UV lamp excited at 365 nm (inset image of Figure 2b). Thus, a ratiometric and colorimetric oxygen nanosensor was realized based on the phosphorescent Pdots.

Using the PL spectral changes, quantitative analysis of oxygen sensing from the ratiometric probe was illustrated by the Stern-Volmer plot as shown in the inset of Figure 2a. Here, we defined R^0_I and R_I as the emission intensity ratios between the phosphorescence at 630 nm and fluorescence at 450 nm in the absence and presence of oxygen, respectively. The Stern-Volmer equation is shown as follows:[11a]

$$R^0_I/R_I = 1 + K_{SV}\, p_{O_2}$$

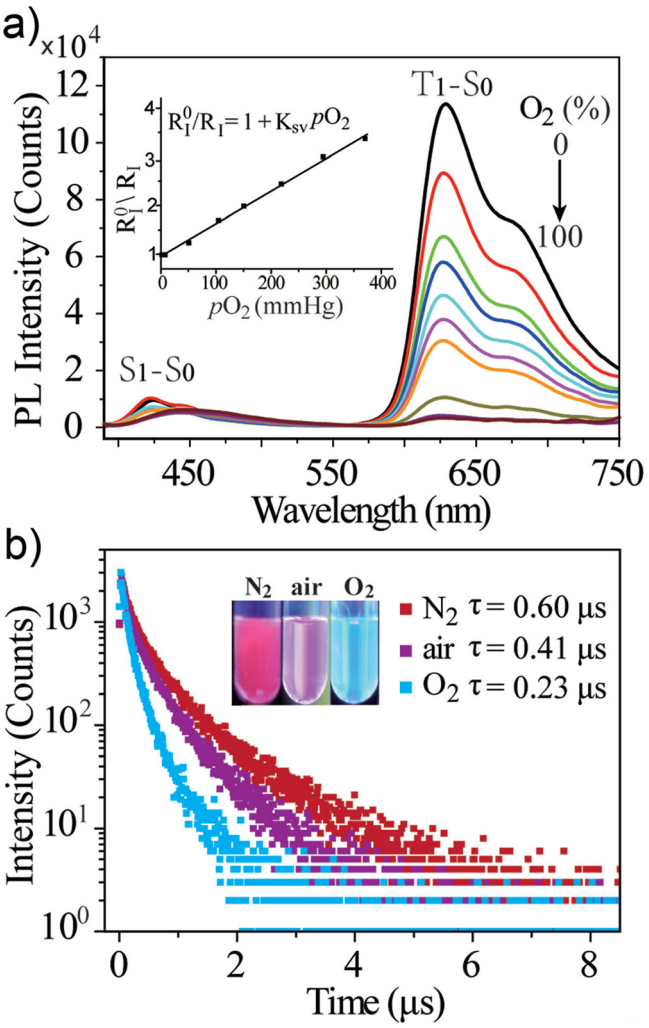

Figure 2. a) PL spectra of WPF-Ir8 in 10 mM PBS solution under different oxygen pressures. Inset: Stern–Volmer plot and linear correlation of the ratiometric fluorescent/phosphorescent response to O_2 partial pressure; b) Fluorescence decays of WPF-Ir8 in aqueous solution saturated with N_2, air and O_2, respectively. Inset: emission images of WPF-Ir8 in aqueous solution saturated with N_2, air and O_2.

where K_{SV} is the Stern-Volmer constant, and p_{O_2} is the oxygen partial pressure. From the trend line in the inset of Figure 2a, a good linear relationship between R^0_I/R_I and p_{O_2} was presented. Based on the slope of the trend line, K_{SV} was estimated to be 6.3×10^{-3} mmHg. By using the K_{SV} value, the oxygen concentration in unknown aqueous solution in the range of 0–50% oxygen level can be detected through the optical response.[15]

To study the oxygen quenching efficiency, the PL spectra of WPF-Ir8 in aqueous solution saturated with N_2 and O_2 were measured (Figure S3 in the SI). According to the following equation: [10]

$$Q = (R_{N_2} - R_{O_2})/R_{N_2}$$

where Q is the oxygen quenching efficiency, and R_{N2} and R_{O2} are the emission intensity ratios between phosphorescence at 630 nm and fluorescence at 450 nm for the WPF-Ir8 solution

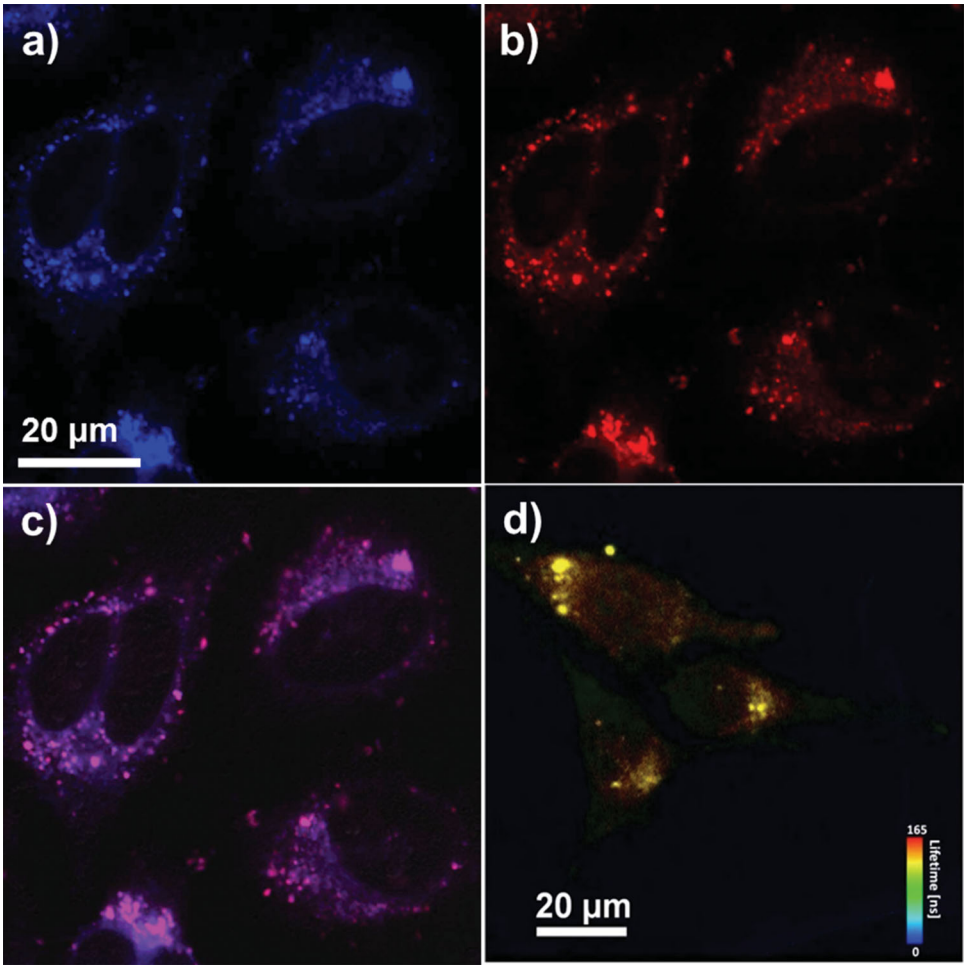

Figure 3. Confocal images of HeLa cells collected at a) 420–460 nm and b) 600–650 nm, c) overlay image of (a) and (b), and d) fluorescent lifetime imaging. The excitation wavelength was 405 nm. HeLa cells were incubated with 7.5 μM WPF-Ir4 at 37 °C for 12 h.

saturated with N_2 and O_2, the Q value was estimated to be 0.967, suggesting high sensitivity of WPF-Ir8 for oxygen as compared with previous report.[10] As a control, we also synthesized the polyfluorene polymer (PFP) without the phosphorescent Ir(III) complex (Scheme S3). Simultaneously, the same experiment was carried out for PFP in aqueous solution (Figure S4 in the SI), and around 30% spectral decrease under oxygen atmosphere was detected, indicating dominant role of the Ir(III) complex in oxygen sensing.

The lifetimes of phosphorescent emission at 630 nm for the Pdots solution in different gas atmosphere were obtained based on the fluorescence decay as shown in Figure 2b. The emission lifetimes at 630 nm for the Pdots aqueous solution saturated with N_2, air and O_2 decreased from 0.60 μs to 0.23 μs, which further confirmed the potent phosphorescence quenching by molecular oxygen.

2.3. Cellular Imaging

In order to demonstrate the application potential of phosphorescent Pdots in PDT, cellular imaging experiments were conducted by a confocal laser scanning microscopy (CLSM), the photodynamic cytotoxicity was evaluated by (3-(4,5-dimethylthiazol-2-yl)-2,5-diphenyltetrazolium bromide (MTT) assay, and the cell apoptosis was studied through flow cytometry technique.

The confocal images of HeLa cells (human cervical carcinoma cells) after incubation with Pdots (WPF-Ir4 at 7.5 μM) in 10 mM PBS at pH 7.0 are shown in **Figure 3** and Figure S6 in the SI. The emission collected at 420–460 nm is assigned to the fluorescence from polyfluorene segment (Figure 3a), and that at 600–650 nm is due to phosphorescent Ir(III) complex (Figure 3b). From the overlay image (Figure 3c), both the blue and red luminescence was observed from the cell cytoplasm, indicating that the Pdots can pass across the cell membrane and enter into the cytoplasm. Although considerable Pdots were endocytosed by HeLa cells, we observed the differentiation of the cells, demonstrating the healthy status of the cells in the presence of Pdots. The low cytotoxicity was further proven by the MTT assay. To highlight the long emission lifetime of phosphorescent Pdots (τ = 0.41 μs in aqueous solution), the fluorescence lifetime imaging microscopy (FLIM) was applied. As shown in Figure 3d and Figure S7, a high-quality long emission

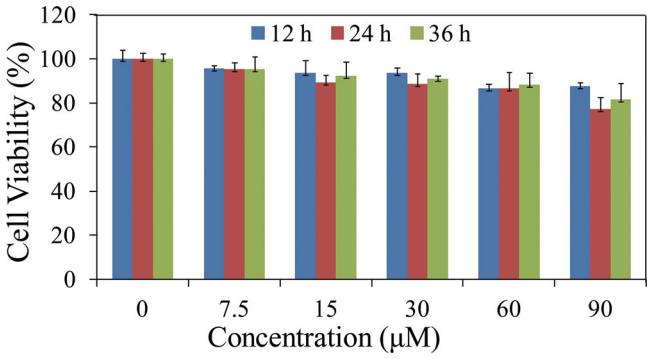

Figure 4. MTT cell viability values (%) of HeLa cells incubated with WPF-Ir4 at various concentrations for 12, 24, and 36 h.

lifetime signal (τ = 150 ns) was observed, which allowed the phosphorescent Pdots to be recognized from the short-lived fluorescent background interferences in the complicated media.

To evaluate the cytotoxicity of the Pdots in living cells, standard MTT assay was carried out for Pdots (WPF-Ir4) in different concentrations. Cell viability values (%) were assessed by MTT proliferation test versus incubation concentrations of Pdots (0–90 μM) in living HeLa cells at 37 °C for 12, 24, and 36 h (**Figure 4**). The cell viability was more than 80% for very high concentration of Pdots (90 μM) after incubation for 36 h. Thus, both the confocal images and MTT assay results indicate that the Pdots have low cytotoxicity and fine biocompatibility for biological applications.

2.4. Photodynamic Therapy

Upon photoexcitation, an energy transfer between the triplet state of the Ir(III) complex in the Pdots and the ground state of molecular oxygen could lead to the generation of an electronically excited state of molecular oxygen, that is, singlet oxygen ($^1O_2$), the process which is called triplet-triplet annihilation (TTA) mechanism.[16] The photogenerated $^1O_2$ is able to kill cancer cells under the PDT process.[17] Thus, the phosphorescent Pdots we studied in this work were further applied as a photosensitizer in PDT for cancer therapy. A chemical trap, 2,2′-(anthracene-9,10-diylbis(methylene)) dimalonic acid (ADMA, Scheme S2),[18] was utilized to capture $^1O_2$ photogenerated by the Pdots. When $^1O_2$ is produced from the system, the photodegradation of ADMA is revealed by its absorption spectral quenching.[19] Therefore, the $^1O_2$ generation efficiency can be indirectly measured by monitoring the absorption spectral changes of ADMA. The experiment was conducted for Pdots (WPF-Ir4, 15 μM) in 10 mM PBS solution containing ADMA (50 μM). The absorption spectra were recorded at ten-minute intervals under irradiation at 488 nm, and the ratios of absorbance between Pdots at 375 nm and ADMA at 259 nm were plotted as a function of the irradiation time. As shown in **Figure 5**a, upon the irradiation, the absorbance at 259 nm assigned to ADMA decreased remarkably, while the one at 375 nm attributed to the Pdots showed negligible changes. The common logarithm of the ratios between the absorbance at 375 nm and 259 nm was taken to investigate the relative $^1O_2$ photogeneration efficiency upon irradiation time from 0 to 50 min. As shown in the inset plot of Figure 5a, $^1O_2$ was generated efficiently with a linear relationship upon the photoexcitation of the Pdots in PBS buffer solution.

The capability of the Pdots for photogenerating $^1O_2$ was expected to induce the oxidative cellular damage and cancer cell death. HeLa cells were chosen as a model to study the PDT effect in vitro. The photodynamic cytotoxicity was evaluated by the MTT assay for Pdots (WPF-Ir4) at various concentrations (0–30 μM). The HeLa cells were first incubated with the Pdots for 12 h. After changing the old medium, the cells were exposed to a light at 488 nm with the irradiation power as low as 2.5 mW cm^{-2} for 30 min. The MTT assay was performed after another 24 h incubation. As shown in Figure 5b, a prominent photocytotoxicity was revealed under the PDT process. At a concentration of 7.5 μM used for the Pdots, the cell death rate reached around 50%. Upon increasing the sample concentration to more than 15 μM, the cell viability decreased to less than 20%. Further prolonging the light exposure time to one hour at 488 nm caused little increase of the cell death rate (Figure S8 in the SI).

To evaluate the photostability of the Pdots and the $^1O_2$ detector ADMA, PL spectra were collected for WPF-Ir4 (15 μM) and ADMA under the irradiation at 488 nm for 90 min (Figures S9 and S10 in the SI). Almost no spectral change for the Pdots even after persistent illumination for 90 min was observed, indicating its high photostability. For ADMA, its absorption and PL spectra kept stable after 90 min of irradiation (Figure S10). In the dark control and light control without any Pdots, the morphologies of HeLa cells maintained normal (**Figure 6**a). After incubation with Pdots (15 μM) upon light irradiation, however, the cell morphologies changed dramatically, showing the cell membrane breach, cytoplasm and nuclear condensation, and a large amount of floating dead cells in the media. As a control, the same experiments were conducted using the PFP without phosphorescent Ir(III) complex (Scheme S3) for cell imaging and PDT. First, the

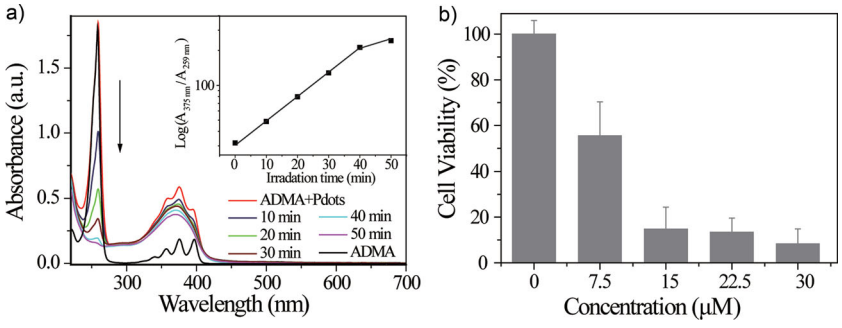

Figure 5. a) Absorption spectra of single oxygen trap ADMA (50 μM) alone, and ADMA (50 μM) with Pdots (15 μM) in 10 mM PBS buffer under irradiation at 488 nm for different times (0–50 min); inset: plot of common logarithm for the absorbance at 259 nm and 375 nm [$\log(A_{375nm}/A_{259nm})$] as a function of light irradiation time in a PBS buffer solution containing WPF-Ir4 (15 μM) and ADMA (50 μM); b) MTT cell viability values (%) of HeLa cells incubated with WPF-Ir4 for 12 h and then irradiated at 488 nm for 30 min.

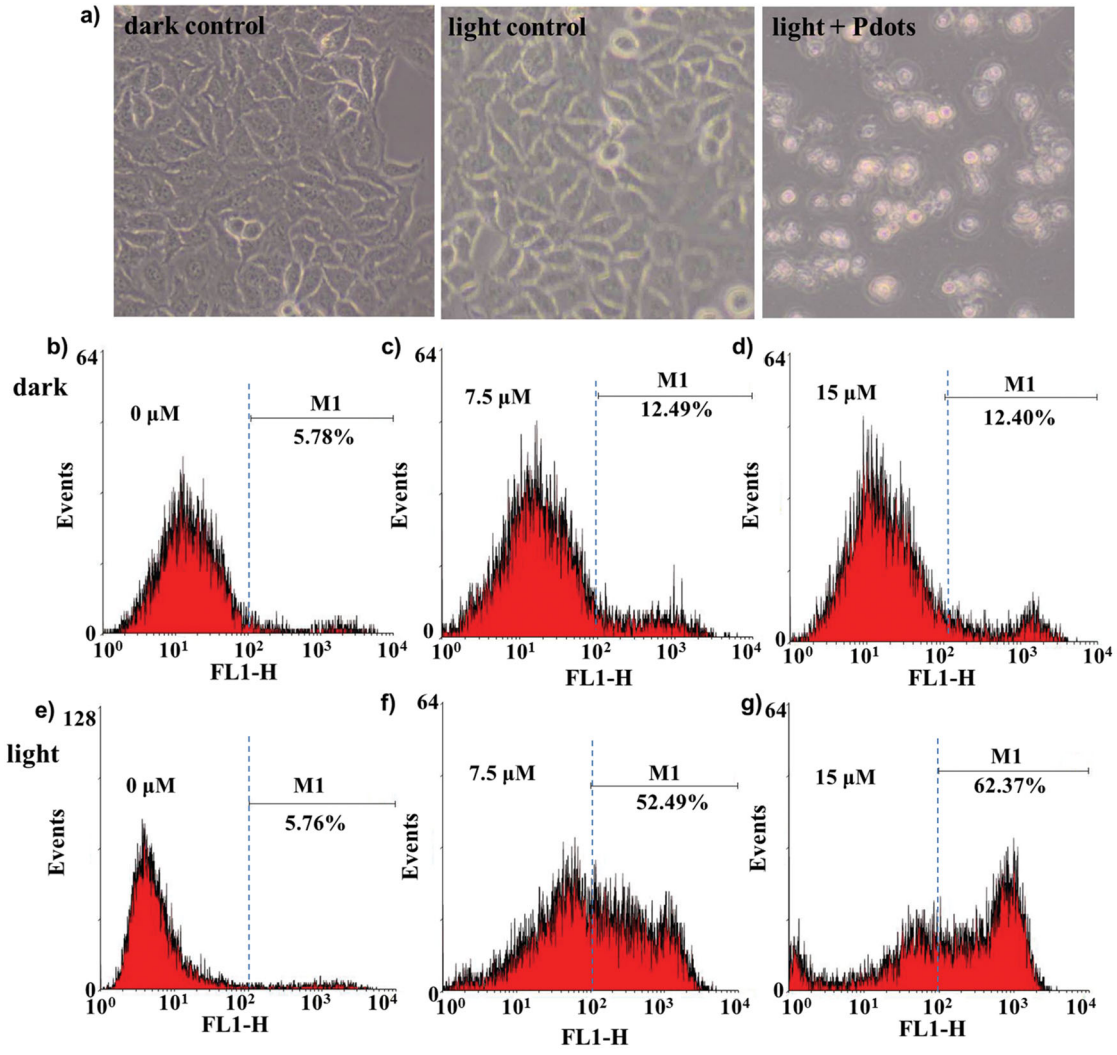

Figure 6. a) Phase contrast bright-field images of HeLa cells in dark control, light control and incubated with the Pdots (15 μM) under irradiation at 488 nm for 30 min. Flow cytometry of HeLa cells incubated with the Pdots (0–15 μM) at 37 °C for 24 h. Hela cells were b–d) in the dark control and e,g) irradiated at 488 nm for 30 min. FL1-H: Annexin V-FITC fluorescence intensity.

$^1O_2$ photogenerated by PFP under irradiation at 405 nm for 90 min was monitored in the presence of ADMA. As shown in Figure S11, the $^1O_2$ generation efficiency by PFP was quite low. Then, PFP (30 μM) was incubated with HeLa cells for 12 h, and then confocal images were taken as shown in Figure S12. The emission collected at 420–460 nm was assigned to the PFP fluorescence. From the overlay image, it was observed that PFP could pass across the cell membrane and label the cytoplasm. Furthermore, the photodynamic cytotoxicity of PFP was conducted by MTT assay under the same PDT procedure used for the phosphorescent Pdots. As shown in Figure S13, the cell viability was more than 70% under the irradiation at 405 nm for 60 min, indicating that the PFP itself showed low photocytotoxicity for living HeLa cells. These results demonstrate that the phosphorescent Pdots explored could be used as a promising anticancer agent under PDT.

To further confirm the anticancer activity of the phosphorescent Pdots as well as to quantify the cell apoptosis, flow cytometry experiments were carried out. Living HeLa cells were incubated with the Pdots (WPF-Ir4) at two concentrations (7.5 μM and 15 μM) for 12 h. After irradiation at 488 nm for 30 min, the cells were cultured for another 24 h. Before the flow cytometry analysis, the cells were stained by Annexin V-FITC cell apoptosis kit. Annexin V-FITC was used to stain the apoptotic cells, where it could bind with phosphatidylserine (PS), a protein located on the cytoplasmic surface of normal cell membrane, but translocated to the outside surface of cell membrane during the cell apoptosis process. Thus, the normal cells present weak or no green fluorescence after staining, while Annexin V-FITC binds with the exposed PS in apoptotic cells to cause higher green fluorescence intensity from the apoptotic cells. HeLa cells without any treatment were used as the blank control. For blank dark control group, the cells were incubated in the dark, while for blank light control group, the cells were exposed to light irradiation at 488 nm for 30 min. In blank dark control and light control groups, cells were also

stained with Annexin V-FITC under the same procedure. After the PDT and staining experiments were conducted followed by 24 h incubation, the cells might be in different apoptotic stages. Because the apoptosis process is a continuous process, the cells at different apoptotic stages could all be observed. For early apoptotic cells, less PS would be translocated to result in weak green fluorescence. For late apoptotic cells, more translocated PS led to higher green fluorescence intensity. As seen from Figure 6b,e, the apoptotic cells were only 5.78 and 5.76% in blank dark and blank light control groups. For the dark control groups with the Pdot samples, the apoptosis rates were around 12% (Figure 6c,d). Significantly, the apoptosis rates reached over 50% for the sample groups upon irradiation for 30 min (Figure 6f,g). These results indicate that the Pdots can effectively induce the apoptosis and lead to the cell death through the PDT process.

3. Conclusions

In summary, a novel type of phosphorescent polymer dots containing the Ir(III) complex have been developed. An efficient energy transfer from the polymer main chain to the phosphorescent Ir(III) complex has been observed in the system. Interestingly, the polymer dots could serve as an optical probe for monitoring oxygen in aqueous solution with a high sensitivity, which could be visualized by naked eyes. The energy transfer in the triplet-triplet annihilation process enables the $^1O_2$ generation, causing effective apoptosis and death of cancer cells under the photodynamic therapy process. To our best knowledge, this is the first example by using single-component phosphorescent polymer dots to carry out the photodynamic therapy in cancer therapy. Thus, this study may provide a new platform for designing multifunctional polymer nanoparticles towards biosensing, imaging and therapy applications in the future.

4. Experimental Section

Materials and Methods: All chemical reagents, unless otherwise specified, were purchased from Sigma Aldrich Chemical Company. All solvents for reactions and photophysical investigations were of HPLC grade. $IrCl_3{\cdot}3H_2O$ was an industrial product and used without further purification. The polymer concentrations were determined by the molecular weight of the polymer repeat unit (RU), which was calculated through the feed ratios of the polymers. Taking WPF-Ir4 as an example: its molecular weight is 679.0 g mol^{-1}, including 0.04 mol Ir(III) complex unit and 0.96 mol fluorene unit. Stock solutions for the polymers (1 mM) were prepared in MilliQ water, which were diluted to different concentrations in 10 mM PBS solution. Photoluminescence (PL) and PL excitation spectra were measured on a Shimadzu RF5300 with Xe lamp excitation source and Edinburgh FL 920 instrument. The UV-vis absorption spectra were recorded on a UV-3600 Shimadzu UV-vis spectrophotometer. The nuclear magnetic resonance (NMR) spectra were recorded on Bruker ACF400 (400 MHz) instrument. Mass spectra were obtained on a Bruker autoflex matrix-assisted laser desorption ionization time-of-flight (MALDI-TOF/TOF) mass spectrometer (MS3) and a Shimadzu GCMS-QP2010. The gel permeation chromatography (GPC) analysis of the polymers was conducted on a Shimadzu 10 Å with THF as the eluent and poly(styrene) as the standard. The data were analyzed by using the software package provided by Shimadzu Instruments. Photographs of the solution samples were taken by a Cannon EOC 400D Digital camera under a hand-held UV lamp excited at 365 nm. Hydrodynamic diameter was determined by dynamic light scattering (DLS) with particle sizing software (90 plus, Brookhaven Instruments Co. USA) at a fixed angle of 90° at room temperature. Zeta potential was measured by Zeta-plus zeta potential analyzer. Phosphorescence lifetimes were determined by an Edinburgh instrument laser impulse fluorometer with picosecond time resolution. High resolution transmission electron microscopy (HR-TEM) images were taken by JEOL 2010 TEM at 200 kV. A microplate reader (infinite 200 PRO, Tecan) was employed for the (3-(4,5-dimethylthiazol-2-yl)-2,5-diphenyltetrazolium bromide (MTT) assay. Confocal microscopy images were taken by a Leica TCS confocal microscope (Nikon, Eclipse TE2000-E, 60 × oil objective). Bright-field images of cells were obtained by an inverted microscope Olympus CKX41. The fluorescent lifetime images were obtained by Olympus IX81 laser scanning confocal microscope. The fluorescence signal was detected by confocal microscope, and correlative calculation of the data was performed by a professional software provided by PicoQuant S19 company. The light from the pulse diode laser head (PicoQuant, PDL 800-D) with excitation wavelength of 405 nm and frequency of 0.5 MHz was used to focuse on the samples with a 40x/NA 0.95 objective lens. Flow cytometry experiments were conducted by BD FACS Calibur Flow Cytometer.

Cell Culture: HeLa cells were cultured in DMEM medium containing 10% FBS (Gibco) and penicillin (1%) at 37 °C under 5% CO_2 atmosphere. The cell culture medium was changed every 48 h.

CLSM: The HeLa cells were seeded into a 6-well plate (Nunc) at an initial cell density of 2×10^4 cells cm^{-2}. After 24 h growth, the cells were treated with the Pdots (15 μM) for 12 h. Then, the cell culture medium was removed and HeLa cells were washed with PBS (pH = 7.4) before fixed by 4.0% formaldehyde (1 mL) at room temperature. The fixed cells were again washed with PBS buffer (pH = 7.4) for three times before observation by confocal laser scanning microscope (60 × oil objective).

MTT Assay: The cytotoxicity of Pdot itself and the photocytotoxicity effect of the Pdots were evaluated by MTT assay. HeLa cells were seeded into a 96-well plate at a density of 1×10^4 cells per well and cultured for 24 h. Pdots were added into each well at a series of concentrations (0, 7.5, 15, 30, 60, and 90 μM). After incubation for 12, 24, and 36 h, respectively, the medium was removed, and the cells were washed by PBS twice to remove free Pdots in the medium. Fresh complete DMEM medium (100 μL) containing MTT (5 mg mL^{-1}) was added into each well. After 4 h incubation, the medium was removed and DMSO (100 μL) was added into each well. The plate was gently shaken for 5 min and the absorbance intensity at 565 nm was recorded using a microplate reader. The relative cell viability related to control wells treated with medium only was calculated by $[A]_{test}/[A]_{control}$, where $[A]_{test}$ and $[A]_{control}$ are the average absorbance of the test and control samples ($n = 8$), respectively.

The photodynamic cytotoxicity experiment was conducted using a similar procedure. HeLa cells were seeded into a 96-well plate and cultured in DMEM for 24 h. Then, the Pdots at a series of concentrations (0, 7.5, 15, 22.5, and 30 μM) were added and incubated for 12 h. Then, the medium was replaced by fresh medium. The cells were further cultured for 4 h before exposure to 488 nm light (2.5 mW cm^{-2}) for 30 min, followed by further incubation for 24 h before the MTT assay.

Cell Apoptosis Assay by Flow Cytometry: HeLa cells were seeded in 6-well plates and grown in complete DMEM medium for 24 h. The Pdots (0, 7.5, and 15 μM) were added into each well. After incubation for 12 h, the medium was removed and fresh complete medium was added. Then, the plates were irradiated at 488 nm laser light (2.5 mW cm^{-2}) for 30 min. After 24 h further incubation, the medium was removed and cells were harvested by trypsin treatment. The collected cells were centrifuged and washed by PBS twice before staining by the apoptosis/death cell assay kit (Invitrogen) according to the product's protocol. Annexin V-FITC was used to stain the apoptotic cells. Finally, flow cytometry analysis was performed by BD FACS Calibur Flow Cytometer.

Supporting Information

Supporting Information is available from the Wiley Online Library or from the author.

Acknowledgements

This work was financially supported by the Singapore National Research Foundation Fellowship (NRF2009NRFRF001–015), the Singapore National Research Foundation CREATE program—Singapore Peking University Research Centre for a Sustainable Low-Carbon Future, and the NTU-A*STAR Centre of Excellence for Silicon Technologies (A*Star SERC No. 112 351 0003). It was also supported by the National Natural Science Foundation of China (No. 21304046 and 21171098).

Received: February 25, 2014
Revised: March 20, 2014
Published online: May 11, 2014

[1] a) J. Pecher, S. Mecking, *Chem. Rev.* **2010**, *110*, 6260; b) C. F. Wu, D. T. Chiu, *Angew. Chem.* **2013**, *125*, 3164; *Angew. Chem. Int. Ed.* **2013**, *52*, 3086; c) K. Li, B. Liu, *J. Mater. Chem.* **2012**, *22*, 1257; d) T. L. Kelly, M. O. Wolf, *Chem. Soc. Rev.* **2010**, *39*, 1526.

[2] a) H. Jiang, P. Taranekar, J. R. Reynolds, K. S. Schanze, *Angew. Chem.* **2009**, *121*, 4364; *Angew. Chem. Int. Ed.* **2009**, *48*, 4300; b) K. Y. Pu, B. Liu, *Adv. Funct. Mater.* **2011**, *21*, 3408; c) C. L. Zhu, L. B. Liu, Q. Yang, F. T. Lv, S. Wang, *Chem. Rev.* **2012**, *112*, 4687; d) A. Duarte, K. Y. Pu, B. Liu, G. C. Bazan, *Chem. Mater.* **2011**, *23*, 501.

[3] a) C. F. Wu, T. Schneider, M. Zeigler, J. B. Yu, P. G. Schiro, D. R. Burnham, J. D. McNeill, D. T. Chiu, *J. Am. Chem. Soc.* **2010**, *132*, 15410; b) J. Pecher, S. Mecking, *Chem. Rev.* **2010**, *110*, 6260; c) Y. H. Chan, F. M. Ye, M. E. Gallina, X. J. Zhang, Y. H. Jin, I. C. Wu, D. T. Chiu, *J. Am. Chem. Soc.* **2012**, *134*, 7309.

[4] a) Y. Sun, W. P. Cao, S. L. Li, S. B. Jin, K. Hu, L. M. Hu, Y. Huang, X. Y. Gao, Y. Wu, X. J. Liang, *Sci. Rep.* **2013**, *3*, 3036; b) Y. H. Chan, F. Ye, M. E. Gallina, X. Zhang, Yu. Jin, I. C. Wu, D. T. Chiu, *J. Am. Chem. Soc.* **2012**, *134*, 7309; c) K. Y. Pu, Ad. J. Shuhendler, J. V. Jokerst, J. G. Mei, S. S. Gambhir, Z. N. Bao, J. H. Rao, *Nat. Nanotechnol.* **2014**, *9*, 233.

[5] a) Q. Zhao, F. Y. Li, C. H. Huang, *Chem. Soc. Rev.* **2010**, *39*, 3007; b) C. L. Ho, W. Y. Wong, *Coord. Chem. Rev.* **2013**, *257*, 1614.

[6] Q. Zhao, C. H. Huang, F. Y. Li, *Chem. Soc. Rev.* **2011**, *40*, 2508.

[7] a) Y. You, S. Lee, T. Kim, K. Ohkubo, W. S. Chae, S. Fukuzumi, G. J. Jhon, W. Nam, S. J. Lippard, *J. Am. Chem. Soc.* **2011**, *133*, 18328; b) Y. Tang, H. R. Yang, H. B. Sun, S. J. Liu, J. X. Wang, Q. Zhao, X. M. Liu, W. J. Xu, S. B. Li, W. Huang, *Chem. Eur. J.* **2013**, *19*, 1311.

[8] C. Shi, H. B. Sun, X. Tang, W. Lv, H. Yan, Q. Zhao, J. X. Wang, W. Huang, *Angew. Chem.* **2013**, *125*, 13676; *Angew. Chem. Int. Ed.* **2013**, *125*, 13676.

[9] a) H. F. Shi, H. Sun, H. Yang, S. J. Liu, G. Jenkins, W. Feng, F. Y. Li, Q. Zhao, B. Liu, W. Huang, *Adv. Funct. Mater.* **2013**, *23*, 3268; b) H. F. Shi, X. J. Chen, S. J. Liu, H. Xu, Z. F. An, L. Ouyang, Z. Z. Tu, Q. Zhao, Q. L. Fan, L. H. Wang, W. Huang, *ACS Appl. Mater. Interfaces* **2013**, *5*, 4562.

[10] C. F. Wu, B. Bull, K. Christensen, J. McNeill, *Angew. Chem.* **2009**, *121*, 2779; *Angew. Chem. Int. Ed.* **2009**, *48*, 2741.

[11] a) T. Yoshihara, Y. Yamaguchi, M. Hosaka, T. Takeuchi, S. Tobita, *Angew. Chem.* **2012**, *124*, 4224; *Angew. Chem. Int. Ed.* **2012**, *51*, 4148; b) S. J. Zhang, M. Hosaka, T. Yoshihara, K. Negishi, Y. Iida, S. Tobita, T. Takeuchi, *Cancer Res.* **2010**, *70*, 4490.

[12] R. Lincoln, L. Kohler, S. Monro, H. Yin, M. Stephenson, R. Zong, A. Chouai, C. Dorsey, R. Hennigar, R. P. Thummel, S. A. McFarland, *J. Am. Chem. Soc.* **2013**, *135*, 17161.

[13] a) H. X. Yuan, H. Chong, B. Wang, C. L. Zhu, L. B. Liu, Q. Yang, F. T. Lv, S. Wang, *J. Am. Chem. Soc.* **2012**, *134*, 13184; b) S. O. McDonnell, M. J. Hall, L. T. Allen, A. Byrne, W. M. Gallagher, D. F. O'Shea, *J. Am. Chem. Soc.* **2005**, *127*, 16360; c) B. S. Howerton, D. K. Heidary, E. C. Glazer, *J. Am. Chem. Soc.* **2012**, *134*, 8324.

[14] H. F. Shi, S. J. Liu, H. B. Sun, W. J. Xu, Z. F. An, J. A. Chen, S. Sun, X. M. Lu, Q. Zhao, W. Huang, *Chem. Eur. J.* **2010**, *16*, 12158.

[15] G. Q. Zhang, G. M. Palmer, M. Dewhirst, C. L. Fraser, *Nat. Mater.* **2009**, *8*, 747.

[16] J. Z. Zhao, W. H. Wu, J. F. Sun, S. Guo, *Chem. Soc. Rev.* **2013**, *42*, 5323.

[17] a) C. F. Xing, L. B. Liu, H. W. Tang, X. L. Feng, Q. Yang, S. Wang, G. C. Bazan, *Adv. Funct. Mater.* **2011**, *21*, 4058; b) X. Ma, S. Sreejith, Y. L. Zhao, *ACS Appl. Mater. Interfaces* **2013**, *5*, 12860.

[18] J. Ma, J. Y. Chen, M. Idowu, T. Nyokong, *J. Phys. Chem. B* **2008**, *112*, 4465.

[19] S. Tuncel, F. Dumoulin, J. Gailer, M. Sooriyaarachchi, D. Atilla, M. Durmus, D. Bouchu, H. Savoie, R. W. Boyle, V. Ahsen, *Dalton Trans.* **2011**, *40*, 4067.